ARTICLE
Journal of Cellular Biochemistry 116:2195–2209 (2015)

Journal of Cellular Biochemistry

Post-Translational Modifications of Histones in Human Sperm

Jana Krejčí,[1] Lenka Stixová,[1] Eva Pagáčová,[1] Soňa Legartová,[1] Stanislav Kozubek,[1] Gabriela Lochmanová,[2] Zbyněk Zdráhal,[2,3] Petra Sehnalová,[1] Siarhei Dabravolski,[4] Jan Hejátko,[4] and Eva Bártová[1]*

[1]*Department of Molecular Cytology and Cytometry, Institute of Biophysics, Academy of Sciences of the Czech Republic, v.v.i., Královopolská 135, Brno 612 65, Czech Republic*

[2]*Research Group-Proteomics, Central European Institute of Technology, Masaryk University, Kamenice 753/5, Brno, Czech Republic*

[3]*National Centre for Biomolecular Research, Faculty of Science, Masaryk University, Kamenice 753/5, Brno, Czech Republic*

[4]*Functional Genomics and Proteomics of Plants, Central European Institute of Technology (CEITEC), Masaryk University, Kamenice 753/5, Brno, Czech Republic*

ABSTRACT

We examined the levels and distribution of post-translationally modified histones and protamines in human sperm. Using western blot immunoassay, immunofluorescence, mass spectrometry (MS), and FLIM-FRET approaches, we analyzed the status of histone modifications and the protamine P2. Among individual samples, we observed variability in the levels of H3K9me1, H3K9me2, H3K27me3, H3K36me3, and H3K79me1, but the level of acetylated (ac) histones H4 was relatively stable in the sperm head fractions, as demonstrated by western blot analysis. Sperm heads with lower levels of P2 exhibited lower levels of H3K9ac, H3K9me1, H3K27me3, H3K36me3, and H3K79me1. A very strong correlation was observed between the levels of P2 and H3K9me2. FLIM-FRET analysis additionally revealed that acetylated histones H4 are not only parts of sperm chromatin but also appear in a non-integrated form. Intriguingly, H4ac and H3K27me3 were detected in sperm tail fractions via western blot analysis. An appearance of specific histone H3 and H4 acetylation and H3 methylation in sperm tail fractions was

Abbreviations: ac, acetylated; BSA, bovine serum albumin; DAPI, 4′,6-diamidino-2-phenylindole; DMEM, Dulbecco′s modified Eagle′s medium; DTT, dithiothreitol; EMEM, eagle′s minimum essential medium; FBS, fetal bovine serum; HAT, histone acetyl transferase; HDAC, histone deacetylase; hESCs, human embryonic stem cells; LC-MS/MS, liquid chromatography tandem-mass spectrometry; MS, mass spectrometry; me1/me2/me3, mono-/di-/tri-methylated; PI, propidium iodide; P2, protamine 2; PBS, phosphate-buffered saline; PTMs, post-translational modifications; RIPA, buffer radio-immunoprecipitation assay buffer; SDS, sodium dodecyl sulfate; WB, western blot; WHO, world health organization.

Authors' contributions: JK performed the sperm processing, western blot analysis, laser scanning confocal microscopy, and spinning disk semi-confocal microscopy. JK and LS carried out the immunofluorescence analysis. LS carried out the transmission light microscopy experiments to study sperm mobility and viability. JK and EP obtained informed consent from all of the volunteer donors. EP managed the contract between the research group and the IVF clinic. SL carried out the protein quantification using the ImageJ software. PS and JK prepared samples for the FLIM-FRET analysis. SD and JH performed the FLIM-FRET analyses and quantification. SK was responsible for statistical analyses. GL and ZZ performed the MS analysis. EB was responsible for finalizing the images from the laser scanning confocal microscopy, coordinating the experimental efforts, interpreting the data, and writing the manuscript. All of the authors have read and approved the final version of the manuscript.

Ethical conduct of research: Informed consent was obtained from all the volunteer donors. An agreement regarding sample manipulation and research was signed by the Institute of Biophysics ASCR, v.v.i. and the private surgery and IVF clinic Sanus in Hradec Králové (division in Jihlava), Czech Republic. The Ethics Commission of the Faculty of Medicine, Masaryk University, Brno approved this research in 2010. hESCs were maintained according to the law 227/2006 of the Czech Republic and Ethics Committee agreement No. 616/2012-31.

Grant sponsor: European Regional Development Fund (CEITEC, Proteomics Core Facility); Grant number: CZ.1.05/1.1.00/02.0068; Grant sponsor: European Social Fund; Grant number: CZ.1.07/2.3.00/30.0009.

*Corresponding author: Eva Bártová, Institute of Biophysics, Academy of Sciences of the Czech Republic, v.v.i., Královopolská 135, CZ-612 65, Brno, Czech Republic. E-mail: bartova@ibp.cz

Manuscript Received: 18 December 2014; Manuscript Accepted: 19 March 2015

Accepted manuscript online in Wiley Online Library (wileyonlinelibrary.com): 23 March 2015

DOI 10.1002/jcb.25170 •

also confirmed by both LC-MS/MS and MALDI-TOF MS analysis. Taken together, these data indicate that particular post-translational modifications of histones are uniquely distributed in human sperm, and this distribution varies among individuals and among the sperm of a single individual. J. Cell. Biochem. 116: 2195–2209, 2015.

KEY WORDS: HUMAN SPERM; HISTONES; PROTAMINE P2; EPIGENETICS; MICROSCOPY

INTRODUCTION

In general, nuclear functions are dictated not only by DNA sequences but also by the composition of the entire chromatin structure. Histone modifications and DNA methylation also fundamentally influence the functioning of genomes. Post-translational modifications (PTMs) of histones (H1, H2A, H2B, H3, and H4), such as acetylation, methylation, phosphorylation, and ubiquitination, are crucial for the formation of transcriptionally active and inactive chromatin states [Jenuwein and Allis, 2001; Rice and Allis, 2001; Taddei et al., 2005; Bannister and Kouzarides, 2011]. Specific histone modifications are responsible for compartmentalizing the genome into functionally distinct nuclear domains. The ability of histone PTMs to determine different types of chromatin allows for the regulation of transcription and other nuclear processes, such as replication, splicing, and DNA repair [Armbruster et al., 1983; Kouzarides, 2007; Luco et al., 2010; Polo and Jackson, 2011]. Histone PTMs also regulate embryonic development; therefore, the modification of redundant histones in sperm may set epigenetic patterns that are transferred from generation to generation. Increasing evidence indicates that, in the early stages of spermatogenesis, sperm DNA is structured in association with histones into classical nucleosome core particles similar to those observed in somatic cells. As spermatogenesis proceeds, histones are replaced by specific proteins called transition proteins. These transition proteins are in turn replaced by the protamines P1 and P2 [Ward, 1993; Emery and Carrell, 2006]. Biochemically, protamines are cysteine- or arginine-rich proteins that are responsible for the final condensation of sperm chromatin [Lee and Cho, 1999]. The phosphorylation of protamines facilitates the correct association of these proteins with DNA. Protamine-DNA interactions are also influenced by protamine acetylation or methylation [Brunner et al., 2014]. Notably, the ratio of P1 to P2 is a fundamental indicator of male fertility. A P1/P2 ratio outside the range of 0.8–1.2 (most authors suggest that the ideal ratio is 1:1) increases the probability of chromatin instability and genomic aberrations, which are associated with decreased male fertility [Carrell et al., 2008]. Smoking and oxidative stress have a significant impact on the P1/P2 ratio, which in turn impacts DNA integrity and protamine distribution within spermatozoa, and an optimal state of these factors is the basis of male fertility [Hammadeh et al., 2010]. It has long been known that sperm chromatin is compacted into a highly condensed, doughnut-like structure [Ward, 1993]. Previously, the retention of histones during spermatid elongation was thought to occur as a consequence of disrupted chromatin regulation, leading to infertility. However, 26 new histone PTMs and 11 protamine PTMs were recently identified in mouse sperm using protein top-down tandem mass spectrometry (MS) [Brunner et al., 2014]. The H2B variant TH2B [Zalensky et al., 2002] and ubiquitinated H3 and H4 [Carrell, 2012] were described in human sperm. In mouse sperm, Brunner et al. [2014] documented post-translationally modified histones, including H2BT9p, H2BK117me3, H2BK121me3, and H3R83me1, and confirmed the presence of acetylated (ac) histones H3 and H4, methylated histones H3K4 and H3K9, and tri-methylated H3K27. PTMs, such as the acetylation and ubiquitination of histones, have also been described by other authors [Meistrich et al., 1992; Baarends et al., 1999; Baarends et al., 2000; Govin et al., 2006]. Furthermore, sperm histones can appear in mono-, di-, and tri-methylated forms [Brunner et al., 2014]. Therefore, substantial evidence supports the notion that the integrity of sperm chromatin is regulated not only by protamines but also by specifically modified residual histones. This concept is important for fertilization and the subsequent physiological development of the embryo, especially from the perspective of epigenetic memory and error-free DNA repair [Ward et al., 2000; Morris et al., 2002]. This observation has led to the conclusion that post-translationally modified histones in sperm might represent paternal epigenetic memory and may participate in the epigenetic reprogramming of the zygote [van der Heijden et al., 2008].

Based on this knowledge, we investigated the variability of histone PTMs in human sperm. Our hypothesis addressed how post-translationally modified histones are distributed in human sperm. We asked whether there was a correlation between the level of the protamine P2 and heterochromatin-related histone markers or between P2 and post-translationally modified histones that were characteristics of euchromatin. We analyzed the entire sperm population of a single individual and also compared the histone patterns of sperm samples among different individuals. We studied the localization of histones H3 and H4 and protamines in human sperm head and tail fractions. We examined sperm-specific morphology in relation to selected histone methylation and histone acetylation patterns. We used western blot analysis to investigate the levels of H3K4me1, H3K9me1/me2, H3K9ac, H3K27me3, H3K36me3, H3K79me1, and H4ac in the head and tail fractions of sperm from 17 donors. Using liquid chromatography tandem-mass spectrometry (LC-MS/MS) and MALDI-TOF MS, we attempted to confirm the western blot results. We also performed correlation analyses between the level of the P2 protamine and the levels of H3K9me1/me2, H3K9ac, and H3K27me3. Based on our results, we believe that knowledge of the epigenetic patterns in human sperm can be used to identify factors that contribute to male fertility.

MATERIALS AND METHODS

SPERM PROCESSING, DECONDENSATION OF SPERM NUCLEI, AND IMMUNOFLUORESCENCE ANALYSIS

Human ejaculates were obtained from 17 donors. Four samples were screened by the Centre of Assisted Reproduction (IVF, Sanus, Hradec Králové, division in Jihlava, Czech Republic). These samples were

scored as normospermic according the World Health Organization (WHO) criteria established in 2010. These samples were used as reference specimens for comparison with the sperm from the 13 other volunteers. All the donors were informed that the samples would be used for research purposes, and all the donors provided informed consent.

Ejaculates were mixed with two volumes of phosphate-buffered saline (PBS) and centrifuged at 6,000 rpm for 10 min in an Eppendorf 5804R centrifuge equipped with an F-34-6-38 rotor. Sperm cells were washed in PBS and placed onto microscope slides for immunostaining. The cells were dried and then fixed in 0.5% formaldehyde (Sigma-Aldrich, Prague, Czech Republic) for 5 min to maintain the 3D structures. Sperm head decondensation was performed as described by Zalensky et al. [1993]. Briefly, the decondensation was carried out in 10 mM dithiothreitol (DTT; Sigma-Aldrich) and 0.5 mg/ml heparin (Sigma-Aldrich) for 30 min on ice. The cells were then washed in PBS, permeabilized with 0.5% Triton X-100 (Sigma-Aldrich) in PBS, and incubated in a blocking solution consisting of 4% bovine serum albumin (BSA) in PBS with Tween-20 (PBST) for 1 h at room temperature. The primary antibodies used for the immunofluorescence analysis were as follows: anti-protamine 1 (sc-23108) and anti-protamine 2 (sc-23102) (both from Santa Cruz Biotechnology, Santa Cruz, CA); anti-histone H3 (06-755) and anti-H3K27me3 (07-322) (both from Upstate Biotechnology, Lake Placid, NY); anti-H4ac (382160; Calbiochem, Billerica, MA); anti-H3K4me1 (ab8895, Abcam, Cambridge, UK); H3K36me3 (ab9050, Abcam); and H3K79me1 (ab2886, Abcam). After an overnight incubation with the primary antibodies, the samples were washed in PBS three times for 5 min each and incubated with the appropriate secondary antibodies at room temperature for 2 h. The secondary antibodies used were as follows: Alexa Fluor 488-conjugated donkey anti-goat IgG (A-11055), Alexa Fluor 594-conjugated donkey anti-goat IgG (A-11058), and Alexa Fluor 488-conjugated donkey anti-rabbit IgG (A-21206) (all from Invitrogen, Grand Island, NY). As negative controls, samples were incubated without primary antibody or with rabbit control IgG (ab46540-1, Abcam, Cambridge, UK) prior to incubation with the secondary antibody (Supplementary Fig. 1A, B). The primary antibodies were used at a dilution of 1:100, and the secondary antibodies were used at a dilution of 1:200; antibody dilutions were prepared in PBS containing 1% BSA. Nuclei were counterstained with 4′,6-diamidino-2-phenylindole (DAPI; Sigma-Aldrich), and Vectashield (Vector Laboratories, Burlingame, CA) was used as a mounting medium.

CELL CULTURE

IMR90 human lung fibroblasts, NTERA pluripotent human embryonal carcinoma cells, and U2OS human osteosarcoma cells were purchased from the European Collection of Cell Cultures (Salisbury, UK). IMR90 cells were cultivated in Eagle′s Minimum Essential Medium (EMEM; PAN Biotech, Aidenbach, Germany) supplemented with 10% fetal bovine serum (FBS, PAN Biotech), 2 mM glutamine (Invitrogen), 1% nonessential amino acids (PAN Biotech), and a mixture of 500 U/ml penicillin and 5 mg/ml streptomycin. The culture medium for NTERA and U2OS cells consisted of 85% Dulbecco′s modified Eagle′s medium (DMEM, PAN Biotech), 15% FBS, and antibiotics. For comparison, we used human embryonic stem cells (hESCs; line CCTL-17, derived from clone CCTL-12 and provided by Prof. Petr Dvořák of the Faculty of Medicine, Masaryk University, Brno). hESCs were cultivated in defined mTESR1 medium (#05870; Stem Cell Technologies, Vancouver, BC, Canada) supplemented with 10 ng/ml basic fibroblast growth factor (bFGF; Chemicon International, Temecula, CA) in dishes coated with Corning® Matrigel® hESC-qualified matrix (#354277; Corning, Tewksbury, MA). All the cell lines were cultured at 37°C in a humidified atmosphere containing 5% CO_2. Lymphocytes were isolated from the peripheral blood of donors as described by Bartova et al. [2001]. For the western blot analyses, we also used K562 leukemia cells that were cultivated according to Bartova et al. [2005].

PREPARATION OF SAMPLES FOR WESTERN BLOTTING

For western blot analyses, the sperm samples were washed twice in PBS and then incubated with radio-immunoprecipitation assay (RIPA) buffer (R0278; Sigma-Aldrich) containing protease inhibitors (P8340; Sigma-Aldrich) and phosphatase inhibitors (#524627; Calbiochem-Merck Millipore, Czech Republic). The samples were sonicated three times for 10 s each and then incubated for 30 min at 100°C [Korrodi-Gregório et al., 2013]. Using this approach, sperm heads containing nuclei were separated from the sperm tails [Lee et al., 1995; Kuretake et al., 1996]. The samples were then centrifuged at 12,000 rpm for 20 min at 4°C; supernatants consisted of the sperm tail fraction, while the pellets contained the sperm heads. For western blot analyses of the head and tail fractions, the individual fractions were lysed in an appropriate volume of lysis buffer (20 mM Tris–HCl, pH 7.5, containing 1% SDS, and 10% glycerol). Protein concentrations were determined using the Bio-Rad DC Protein Assay Kit (Bio-Consult Laboratories, s.r.o., Prague, Czech Republic). The lysates were mixed with bromophenol blue (0.01%) and 1% β-mercaptoethanol and incubated for 5 min at 100°C.

WESTERN BLOTTING

For the western blot analysis, 5 μg of total proteins from each sample was separated on a 12% gel by SDS–PAGE. After electrotransfer onto an Immobilon-P polyvinylidene difluoride membrane (Sigma-Aldrich), proteins were detected using the appropriate primary and secondary antibodies and visualized with the ECL Plus reagent (Amersham Pharmacia Biotech/GE Healthcare, Chalfont St. Giles, UK) according to the manufacturer′s instructions. The primary antibodies used were as follows: anti-protamine 2 (sc-23102, Santa Cruz Biotechnology; MW = 15 kDa); anti-H4ac (382160, Calbiochem-Merck Millipore; MW of detected band = 15 kDa); anti-H3K4me1 (ab8895, Abcam; MW = 17 kDa); anti-H3K9me1 (ab9045, Abcam; MW = 17 kDa); anti-H3K9me2 (07-212, Upstate; MW = 17 kDa); H3K9ac (06-942, Upstate; MW = 17 kDa); anti-H3K27me3 (07-449, Upstate; MW = 17 kDa); anti-H3K36me3 (ab9050, Abcam; MW = 17 kDa); anti-H3K79me1 (ab2886, Abcam; MW = 17 kDa); and anti-CD45 (ab10558, Abcam, MW = 155 kDa). Anti-rabbit IgG (A-4914, Sigma-Aldrich) and anti-goat IgG (whole molecule, A-4174, Sigma-Aldrich) were used as secondary antibodies. The primary antibodies were diluted 1:1,000 (with the exception of anti-protamine 1, which was used at a dilution of 1:500) in 10 mM Tris, pH 7.4, containing 100 mM NaCl and 0.05% Tween-

20 (TBST). The conditions were optimized for the binding of each antibody: blocking was performed in buffer containing 2% milk or 2% gelatin, and the membranes were washed with TBST solutions of varying salinity. Histone levels were quantified via densitometry and normalized to the levels of total protein and histone H3. The raw data from the western blots are shown in Supplementary Figures 2 and 3.

IMAGE ACQUISITION AND 3D-ANALYSIS OF HUMAN SPERM

Images of formaldehyde-fixed sperm were acquired using a Nipkow spinning disk-based confocal system consisting of four laser diodes (405 nm, 488 nm, 561 nm, and 640 nm, all adjustable in 1 nm increments) (Andor Technology, Belfast, Northern Ireland). The QLC 100 confocal head (VisiTech International, Sunderland, UK) was connected to a Leica DMRXA epifluorescence microscope equipped with piezo-controlled z-movement (Physik Instrumente, Karlsruhe, Germany). The high-speed scanning system was driven by Aquarium software (created by Assoc. Prof. Pavel Matula, Faculty of Informatics, Masaryk University, Brno). A fully programmable digital CoolSNAP CCD camera (Photometrix, Tuscon, AZ) and a Nikon oil objective (Plan Fluo, Japan) were used. The magnification of the objective lens was 100× (numerical aperture [NA] = 1.3), and the pixel/micron conversion factor was 15 pixels/μm. For the 3D reconstruction of the confocal images in this study, we used 40 optical sections obtained in axial steps of 0.1 μm.

For image analyses, we also used a Leica SP5-X laser scanning confocal microscope. The following settings were applied: 1,024 × 1,024 pixels, 400 Hz, bidirectional mode, four lines, zoom 8–12, with the use of an oil objective (HCX PL APO, 63×, NA = 1.4, Leica, Germany). This microscopy system was specifically used for the observation of sperm morphology, mobility, and viability under transmission light (as mentioned in the Results section).

MASS SPECTROMETRY

The separation of sperm head and tail fractions was performed as described in "PREPARATION OF SAMPLES FOR WESTERN BLOTTING." We utilized a fraction separation methodology modified according to Lee at al. [1995], Kuretake et al. [1996], and Korrodi-Gregório et al. [2013]. Isolation and the characterization of histones H3 and H4 by MALDI-TOF MS was performed as previously described [Cincarova et al., 2012; Legartova et al., 2014], with minor modifications. Briefly, histones were separated using a Dionex UltiMate 3000 HPLC system with an Agilent mRP-C18 high-recovery protein column (0.5 × 100 mm, macroporous C18-bonded, 5 μm C18 silica particles). Histone extracts in solvent A [double-distilled water containing 2% acetonitrile (*v/v*) and 0.3% trifluoroacetic acid (*v/v*)] were injected into the column and separated using a multistep acetonitrile gradient at 70°C with a constant flow rate of 9 μl/min. The concentration of solvent B [double distilled water containing 80% acetonitrile (*v/v*) and 0.3% trifluoroacetic acid (*v/v*)] was increased from an initial concentration of 20% to 40% over 7 min, to 60% over 31 min, and then to 80% over 5 min. A Dionex Probot LC Packings Micro fraction collector was used for the collection of histone H3 and H4 fractions. The fractions were dried in a Savant™ SpeedVac SPD 111 V (Thermo Scientific, Waltham, MA), dissolved in 15 μl of 100 mM ammonium acetate (pH 4) containing 0.8 ng/μl endoproteinase Glu-C (sequencing grade; Roche Diagnostics, Basel, Switzerland) and incubated at 25°C for 90 min. The Glu-C digests were analyzed via MALDI-TOF MS on an Ultraflex III mass spectrometer (Bruker, Billerica, MA). A linear positive mode was used for the detection of mass spectra at an acceleration voltage of 25 kV using 2,000 laser pulses. The external calibration of the mass spectra was performed as previously described [Cincarova et al., 2012].

Sample preparation for LC-MS/MS: 5 μg of each protein extract (w/o fractionation) was used and trypsin digestion was performed (40°C, 2 h). LC-MS/MS analyses were done using RSLCnano system connected on-line to Orbitrap Elite hybrid spectrometer (Thermo Fisher Scientific). Tryptic digests were separated on Acclaim Pepmap100 C18 analytical column (2 μm particles, 75 μm × 500 mm; Thermo Fisher Scientific; 300 nl/min) by the following gradient program (mobile phase A: 0.1% FA in water; mobile phase B: 0.1% FA in 80% acetonitrile): elution started at 1% of mobile phase B and increased from 1% to 35% during the first 30 minutes, then increased linearly to 56% in the next 10 min and finally increased linearly to 80% of mobile phase B in the next 5 min and remained at this state for the last 8 min.

MS data were acquired in a data-dependent strategy selecting up to top 10 precursors based on precursor abundance in the survey scan (350–2,000 m/z). The resolution of the survey scan was 60,000 (400 m/z) with a target value of 1×10^6 ions, one microscan and maximum injection time of 200 ms. HCD MS/MS spectra were acquired with a target value of 50,000 and resolution of 15,000 (400 m/z). The maximum injection time for MS/MS was 500 ms. Dynamic exclusion was enabled for 45 s after one MS/MS spectra acquisition and early expiration was disabled. The isolation window for MS/MS fragmentation was set to 2 m/z.

The analysis of the mass spectrometric RAW data files was carried out using the Proteome Discoverer software (1.4, Thermo Fisher Scientific) with in-house Mascot (2.4.1, Matrixscience). Mascot MS/MS ion searches were done against UniProtKB protein database for *Homo sapiens* taxonomy downloaded at 2014-01-01 or against cRAP contaminant database (downloaded from http://www.thegpm.org/crap/) and in-house histon database in parallel. Mass tolerance for peptides and MS/MS fragments were 10 ppm and 0.05 Da, respectively. Oxidation (M), deamidation (N, Q), acetylation (K, protein N-term), methylation (K, R), dimethylation (K), trimethylation (K), and phosphorylation (S, T) as optional modifications and six enzyme miss cleavages were set for searches against histone database. In case of database search against UniProtKB database for *Homo sapiens* oxidation (M), deamidation (N, Q), acetylation (K, protein N-term), and phosphorylation (S, T) as variable peptide modifications and two enzyme miss cleavages were set. Rank 1 peptides with Mascot expectation value <0.01 and with at least six amino acids were considered. Peptide identifications were manually verified and quantitative data evaluation for selected peptides was done in Skyline quantification software (Skyline 2.6.0.7176). Peptide areas were normalized to areas of unmodified peptides of respective histone.

FLIM-FRET ASSAY

For identification of in situ interaction between Alexa 488-labeled protamine P2 and propidium iodide (PI)-stained DNA or Alexa

488-labeled acetylated H4 and PI-stained DNA we used FLIM-FRET assay. Analysis was performed by the use of the laser scanning confocal imaging system Zeiss LSM 780 on inverted microscope equipped with external In Tune laser (488–640 nm, <3 nm width, pulsed, 1.5 mW) and GaAsP detectors. A Plan-Apochromat 63× oil objective, NA 1.4, was used for imaging the samples. Photon counting module Simple-Tau 150 (compact TCSPC system based on SPC-150) with DCC-100 (Detector Controller Card) (Becker & Hickl GmbH) was coupled to Zeiss LSM 780 system to perform FLIM-FRET assays.

The confocal images of protamine P2 and acetylated histone H4, labelled via Alexa 488-conjugated antibody, were acquired. The specimen was excited with donor excitation wavelength 490 nm, which also partially activates PI. With an appropriate laser power and PMT gain, the confocal donor/acceptor images were obtained. For processing of confocal images, the original Zeiss software was used (ZEN 2012 package). The same cell was excited with donor excitation wavelength 490 nm to generate intensity image and photon counting on B&H Simple-Tau module with original SPCM software. Image analysis was performed with B&H software SPCImage. As analytical approach we used pixel per pixel image analysis fitting model for two component system with fixed second component at 4100 ps; binning parameter = 1. For visualization of interacting and non-interacting molecules we used not only standard intensity image and lifetime image, but also ratios of amplitudes (to improve signal-to-noise ratio). The ratio a_2/a_1 of a FLIM decay is the concentration ratio of non-interacting and interacting donor fraction. The observation of two lifetimes in the spectrum of Alexa 488 was expected: first one, close to 4 ns corresponded to non-interacting fraction of Alexa 488 while the second one characterized by shorter lifetime of Alexa 488 represents interacting molecules. Application of three-component fitting model did not reduce χ-square (χ^2) parameter and calculated amplitude for third component was very low (5–7%). FRET-FLIM efficiency was calculated as a ratio of fluorechromes' lifetimes.

STATISTICAL ANALYSIS

The density of western blot bands was analyzed using ImageJ software (http://imagej.en.softonic.com), and regression analysis was performed using Sigma Plot software, version 13.0 (Systat, San Jose, CA). The 95% confidence intervals are shown in the relevant graphs, and the Pearson's correlation coefficient (r or r^2) was calculated using Sigma Plot software. Critical values for r and N (number of samples) were evaluated according to statistical tables [Rohlf and Sokal, 1993].

RESULTS

NUCLEAR LOCALIZATION PATTERNS OF PROTAMINES AND SELECTED POST-TRANSLATIONALLY MODIFIED HISTONES IN HUMAN SPERM

During sperm development, 85–95% of the histones are removed from chromatin and are substituted with protamines (reviewed in [Jenkins and Carrell, 2012]). Notably, protamines do not replace histones directly. Rather, histones are replaced on spermatid chromatin by so-called transition proteins (T1/T2), which are in turn replaced by protamines (reviewed in [Balhorn, 2007]). In this study, we analyzed the localization patterns of the protamine P2 in parallel with those of the residual histones H3 and H4 in human sperm (Figs. 1 and 2). Immunofluorescence analyses revealed a high level of P2 at the periphery of the sperm nuclei (Fig. 1A, B). However, the sperm nuclei were not decorated with α-tubulin, which was only present in the sperm tails (Fig. 1C, D). Our analyses indicated that the nuclear distribution pattern of P2 is variable in the sperm samples from different individuals and also varied among the sperm from a single individual (Fig. 1A, B). Similar trends were found for histone H3 (Figs. 1B, D, see later in Fig. 2Aa, Ba).

We also studied the nuclear patterns of fundamental PTMs of histones (Fig. 1E–G and Fig. 2). We observed variable levels of H3K9me1 in sperm heads; an example of very low H3K9me1 levels are seen in Figure 1E. Human sperm were also positive for H3K36me3 and H3K79me1 (Fig. 1F, G). From a morphological point of view, we found that H3K4me1 accumulated in a wide strip in the central region of the sperm heads (Fig. 2Aa, Ab, red arrows). In contrast, in other sperm heads from the same individual, two H3K4me1-positive discs were present (Fig. 2Aa, Ab, yellow arrows).

Notably, the localization patterns of H3K27me3 in sperm heads were variable, as indicated by the following: (1) some sperm heads were characterized by a high level of evenly distributed H3K27me3; (2) in some individuals, H3K27me3 was barely detected in large sperm heads (Fig. 2Ba, Bb, asterisk); and (3) the sperm heads of some samples were characterized by an H3K27me3-positive strip (Fig. 2Ba, Bb, yellow arrow). H3K27me3 positivity was also observed at the mid-piece and in the remainder of intact sperm tails, as shown by the immunofluorescence analysis (Fig. 2Ba, Bb, frames show the mid-piece).

H4ac was located in the inner region of sperm heads and at the mid-piece (Fig. 2Ca, Cb, frames). Negative control samples for immunofluorescence are presented in Supplementary Figure 1A, B. The percentages of sperm heads that were positive for selected PTMs of histones in individual donors are shown in Supplementary Table 1.

In this study, we also tested interactions between P2 protamines and DNA and between acetylated histones H4 and DNA using a FLIM-FRET experimental approach (Fig. 3A–D). Very high FLIM-FRET efficiencies were found for P2 and DNA at both (A) the sperm head interior and (B) the sperm head periphery (64.5% and 59.5%, respectively). The FLIM-FRET efficiency is mentioned for the sperm nucleus depicted in Figure 3A, B (the efficiency data are shown for the region labeled with red asterisks in panels Ab, Bb). A lower FLIM-FRET efficiency (39.6%) was found for H4ac and DNA in the internal part of the sperm head (C). However, as seen in (D), the FLIM-FRET efficiency for peripherally positioned acetylated H4 was 65.3% in the depicted image (Fig. 3D; the efficiency measurement is for the region labeled by red asterisks in panel Db). Together, the FLIM-FRET data revealed that a substantial fraction of acetylated histones H4 is integrated into the sperm chromatin. Therefore, these histones likely represent potentially functional epigenetic elements. However, a fraction of the H4ac might be so-called "inactive" remainders of an incomplete histone degradation process. These remainders could appear after the replacement of histones by protamines during

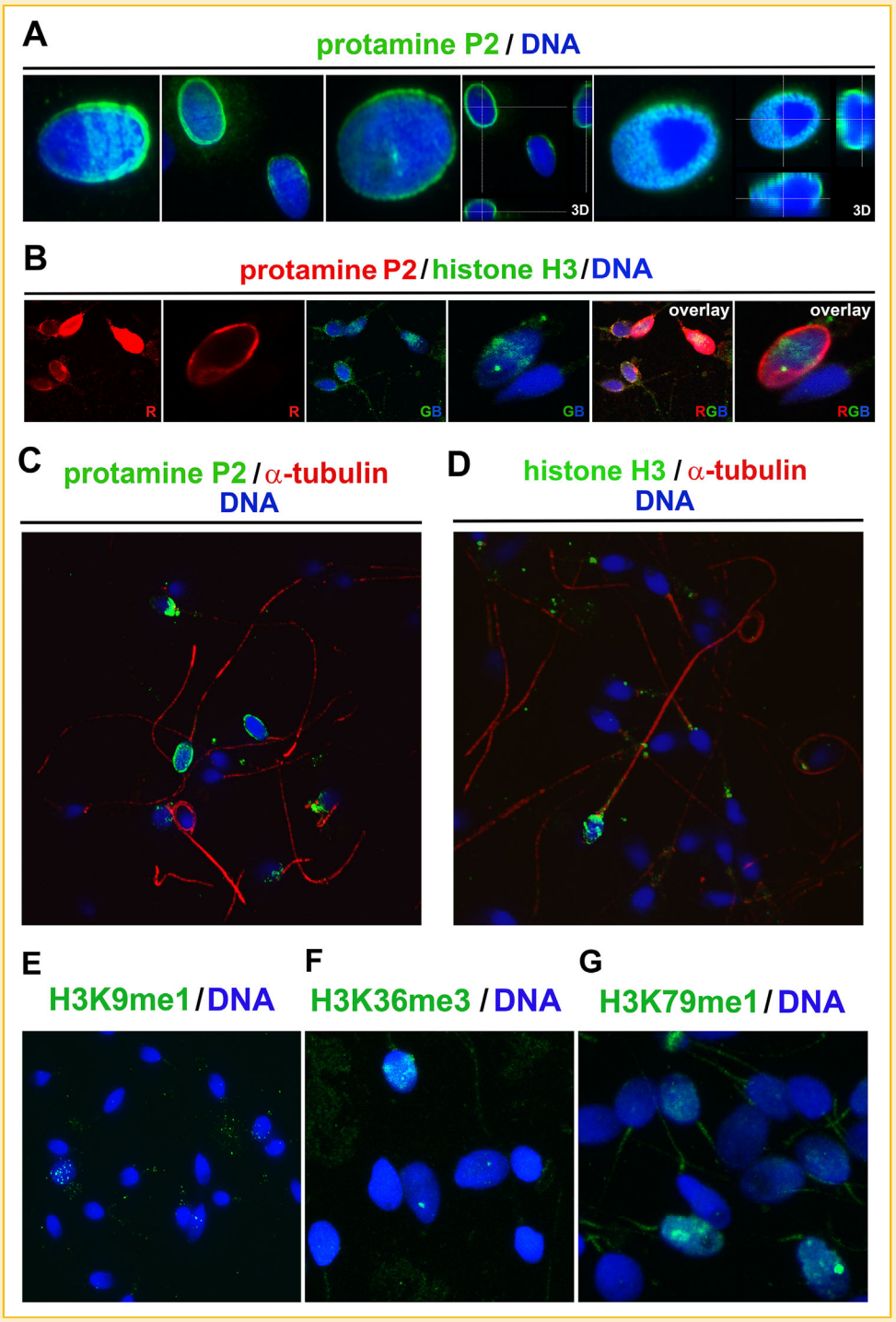

Fig. 1. Localization of P2 and histones in sperm. A: The highest level of P2 (green) was at the periphery of the sperm heads. A 3D reconstruction of confocal images of protamine P2 (green) is shown. B: Morphology of protamine P2 (red) and histone H3 (green) in human sperm. C: Morphology of protamine P2 (green) and α-tubulin (red) in human sperm. D: Morphology of histone H3 (green) and α-tubulin (red) in human sperm. Nuclear patterns of E: H3K9me1, F: H3K36me3, and G: H3K79me1 (all in green). Nuclei (DNA) were counterstained with DAPI (blue).

spermatogenesis (see the non-integrated fraction in the blue region of the graphs in panels Cc and Dc).

The results obtained via immunofluorescence that demonstrated the presence of post-translationally modified histones in the sperm tail fraction we also verified by mass spectrometry (Fig. 4A–C). For detection of PTMs of histones H3 and H4 we used LC-MS/MS analysis (Fig. 4A) and MALDI-TOF MS (Fig. 4B, C). LC-MS/MS analysis indicated that head/tail peptide area ratio for R.

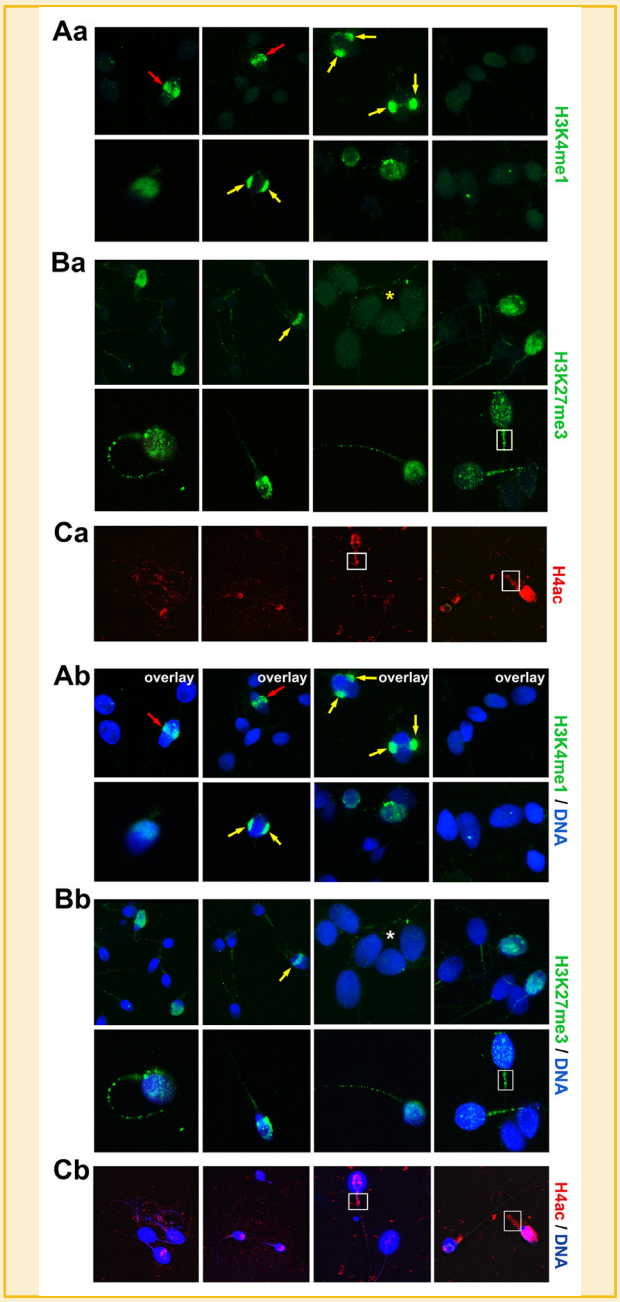

Fig. 2. Variability in post-translationally modified histones in human sperm. Immunofluorescence analyses of A: H3K4me1 (green), B: H3K27me3 (green), and C: H4ac (red) in human sperm. Panels Aa, Ba, and Ca show fluorescence in the green or red regions of the spectra. Panels Ab, Bb, and Cb show green–blue or red–blue overlays. Nuclei were counterstained with DAPI (blue). Panel A: A strip-like pattern (red arrows) or the accumulation into two symmetrically located disk-like structures (yellow arrows) was observed for H3K4me1. Panel B: H3K27me3 was present in sperm heads. A robust H3K27me3-positive strip was observed in some sperm heads (B, yellow arrow). In some samples, H3K27me3 was absent from the sperm (B, asterisk shows only autofluorescence). In other individual samples, some sperm heads were strongly positive for H3K27me3. Panel C: H4 acetylation (red) was observed in sperm heads (blue). The localization patterns of post-translationally modified histones were variable among the sperm heads (nuclei) and among samples from different individuals. Fluorescence signals for H3K27me3 and H4ac were observed in the mid-piece (white frames in panels B and C).

K9me2STGGK14acAPR.K and R.KQLATK24acAAR.K is significantly lower on histone H3 of sperm heads when compared with sperm tail fraction (Fig. 4Aa, head to tail ratios are shown). In case of all forms of peptide R.K9 meXSTGGK14acAPR.K (X = 2 – 3) we always detected both modification sites together and it is not possible to assign changes in peptide level to particular modification. In contrast, quantitatively higher multiple-acetylated forms R.GKGGKGLGKGGAKR.H were found on H4 in sperm head fraction (Fig. 4Ab, asterisks). Di-, tri-, and tetra-acetylated forms of histone H4 in sperm tail fraction were detected only by LC-MS/MS due to lower sensitivity of MALDI-TOF MS.

MALDI-TOF-MS analysis of three independent biological replicates revealed differences in H4 acetylation (compare Fig. 4Ca, Cb). In the case of H4, highly modified N-terminal peptides represented the dominant forms of H4 in the sperm heads and a different acetylation pattern of H4 was observed in two separated fractions (compare peaks in Fig. 4Ca, Cb). In addition, indication of changes in histone H3 methylation and acetylation states in the sperm tail and head fractions were observed (Fig. 4Ba, Bb).

To disprove or confirm the infiltration of somatic cells, such as lymphocytes, (characterized by a high level of histone PTMs) into the sperm tail fraction, we performed a western blot analysis with an antibody directed against CD45, a marker of nucleated hematopoietic cells, as described previously [Tunc and Tremellen, 2009]. In this test, both sperm fractions were negative (Fig. 5A). Therefore, we believe that the PTM of histones occurs not only in sperm heads but also in the tail fractions, and these samples were not contaminated by somatic cells due to methodological imperfections (Figs. 5A, B and 6B–E).

DIFFERENCES IN POST-TRANSLATIONALLY MODIFIED HISTONES IN SPERM SAMPLES FROM DIFFERENT INDIVIDUALS

We used western blotting to analyze the levels of P2 in spermatozoa from four normospermic donors, as specified by renowned IVF clinics. The same analysis was also performed for H3K4me1, H3K9me1/me2, H3K27me3, H3K36me3, H3K79me1, H4ac, and total histone H3 (Fig. 5B). We compared the levels of selected proteins in human sperm, hESCs, NTERA, and IMR90 cells. The levels of H3K4me1 and H4ac were identical in hESCs and the sperm head fractions of three normospermic individuals (samples labeled donors D2–D4). However, the H3K4me1 level was lower in sample D1. In addition, the levels of H3K9me1 were lower in the sperm heads of individuals D2–D4 compared to those in hESCs or NTERA or IMR90 cells (Fig. 5B). Sample D1 was characterized by the absence or very low levels of H3K9me1 and H3K9me2 (Fig. 5B, asterisks). Notably, levels of the heterochromatin marker H3K27me3 were higher in the sperm head fractions of the normospermic donors (D1–D4) than in hESCs and NTERA and IMR90 cells (Fig. 5B). The presence of H3K27me3 may be linked to high chromatin compaction in the sperm. This heterochromatinization might signify a defense mechanism in response to potential sperm DNA damage [Aoki et al., 2006].

We also investigated whether the PTMs of histones can occur in sperm tail fractions. We found by western blots that sperm tails are very highly positive for H3K27me3 and H4ac. However, no H3K4me1, H3K9me1/me2, H3K36me3 or H3K79me1 was observed in the tail fractions of any of the samples analyzed (Fig. 5B). Total histone H3 was barely detected in the tail fractions of samples D1,

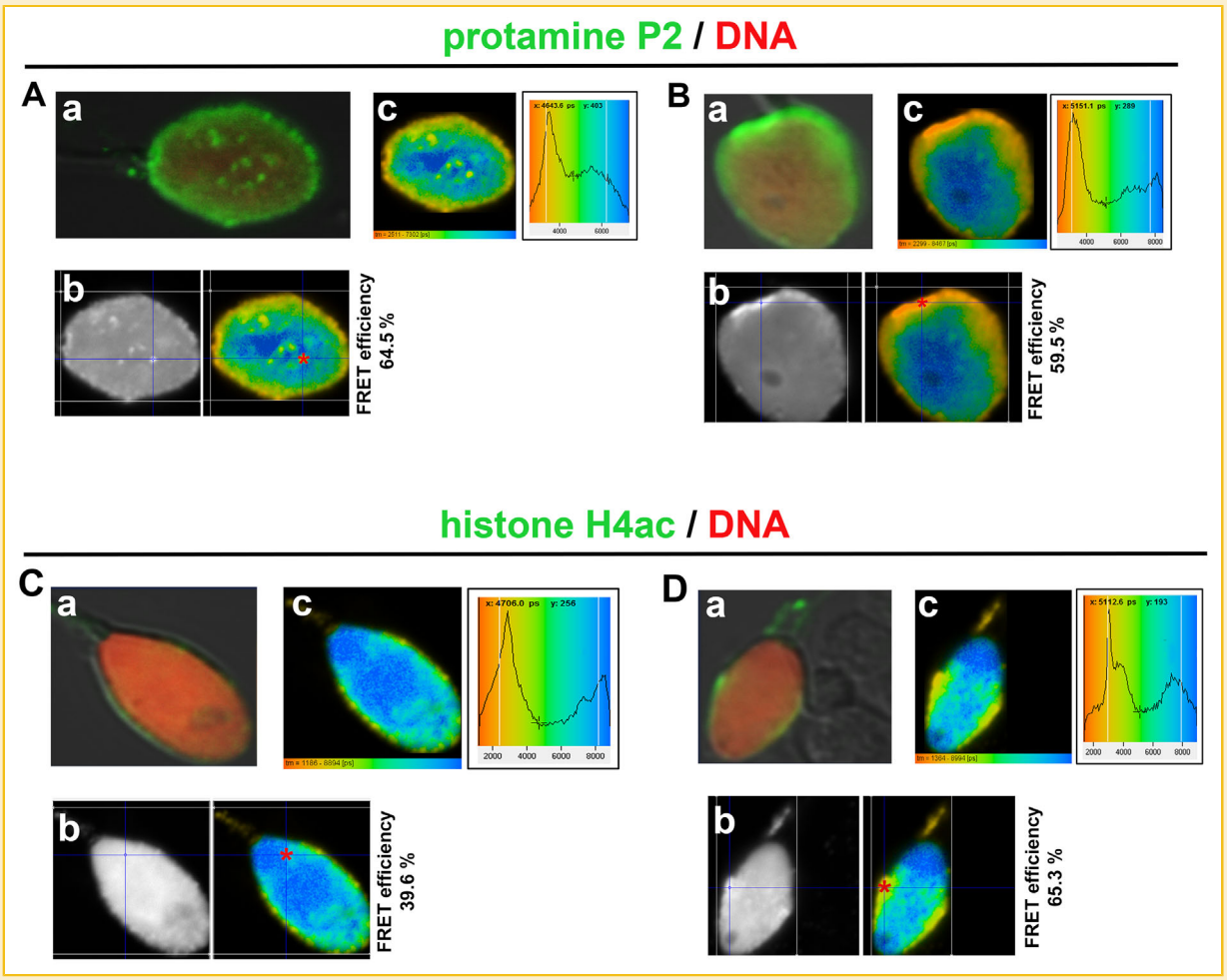

Fig. 3. Degree of integration of protamine P2 or acetylated histone H4 into sperm chromatin. For the FLIM-FRET experiments, Alexa-488 was used to stain protamine P2 (or histone H4ac). The DNA was visualized using propidium iodide. The lifetime of Alexa 488 is 4,100 ps. If proteins interact, the lifetime decreases to 2,000–3,000 ps. Studies were performed to assess the following interactions: Panels A–B, protamine P2 and DNA, and C–D, histone H4ac and DNA. Panels (a) indicate the visualization (confocal image) of sperm heads using the ZEN software (Zeiss). Panels (b) and (c) show the quantification of the protein-DNA interactions using the SPCM software. A: Measurement of the P2-DNA interaction in the internal part (red asterisks) of the sperm head (nucleus). B: Measurement of the P2-DNA interaction at the periphery (red asterisk) of the sperm head. C: Measurement of the H4ac-DNA interaction in the internal part (red asterisks) of sperm head. D: Measurement of the interaction between H4ac and DNA at the periphery (red asterisk) of sperm head. Red asterisks indicate selected pixels where the FLIM-FRET efficiency was calculated. Pictures in panels (c) represent single image measurements, and the histograms showing the mean fluorescence lifetime distribution (average of lifetimes of the components of the multi-exponential decay weighted by their amplitude coefficients [corresponding to the amount of molecules] are enclosed). In the charts, the peaks in the red areas of the spectra represent interacting molecules.

D2, and D4, but sample D3 was characterized by H3 positivity in the tails, which fits well with H3K27me3 positivity; also high in sample D3 (Fig. 5B).

With respect to histone modification patterns, the clinically normospermic sample D1, in particular, differed from samples D2–D4 (Fig. 5B, asterisks). Sperm from the D1 individual were characterized by a high level of P2, similar to the P2 levels found in samples D2–D4, whereas the levels of H3K4me1, H3K36me3, and H3K79me1 were lower and H3K9me1 and H3K9me2 were barely detectable in the D1 sample compared with samples D2–D4 (Fig. 5B, asterisks). These results demonstrate that it is important to analyze not only the protamine levels but also the histone profiles when evaluating normospermia.

Next, we examined the sperm samples of 13 volunteers in detail (Fig. 6A). In these samples, we first tested the cellularity of the ejaculate (cell number/ml), total cell count, and sperm viability. These parameters were highly variable among individuals (Fig. 6A). In these samples, we separated the sperm head and tail fractions and performed additional western blot analyses (Fig. 6B–E). These analyses demonstrated again variability in the levels of H3K4me1, H3K9ac, H3K9me1/me2, H3K27me3, and to a lesser extent H4ac in the sperm heads of the 13 donor samples when normalized to the total histone H3 levels (Fig. 6B, D). Among the samples from different individuals, pronounced variability in the level of H3K9me1 was found in the sperm head fractions: some samples were characterized by very high level of H3K9me1, but some samples were absent of

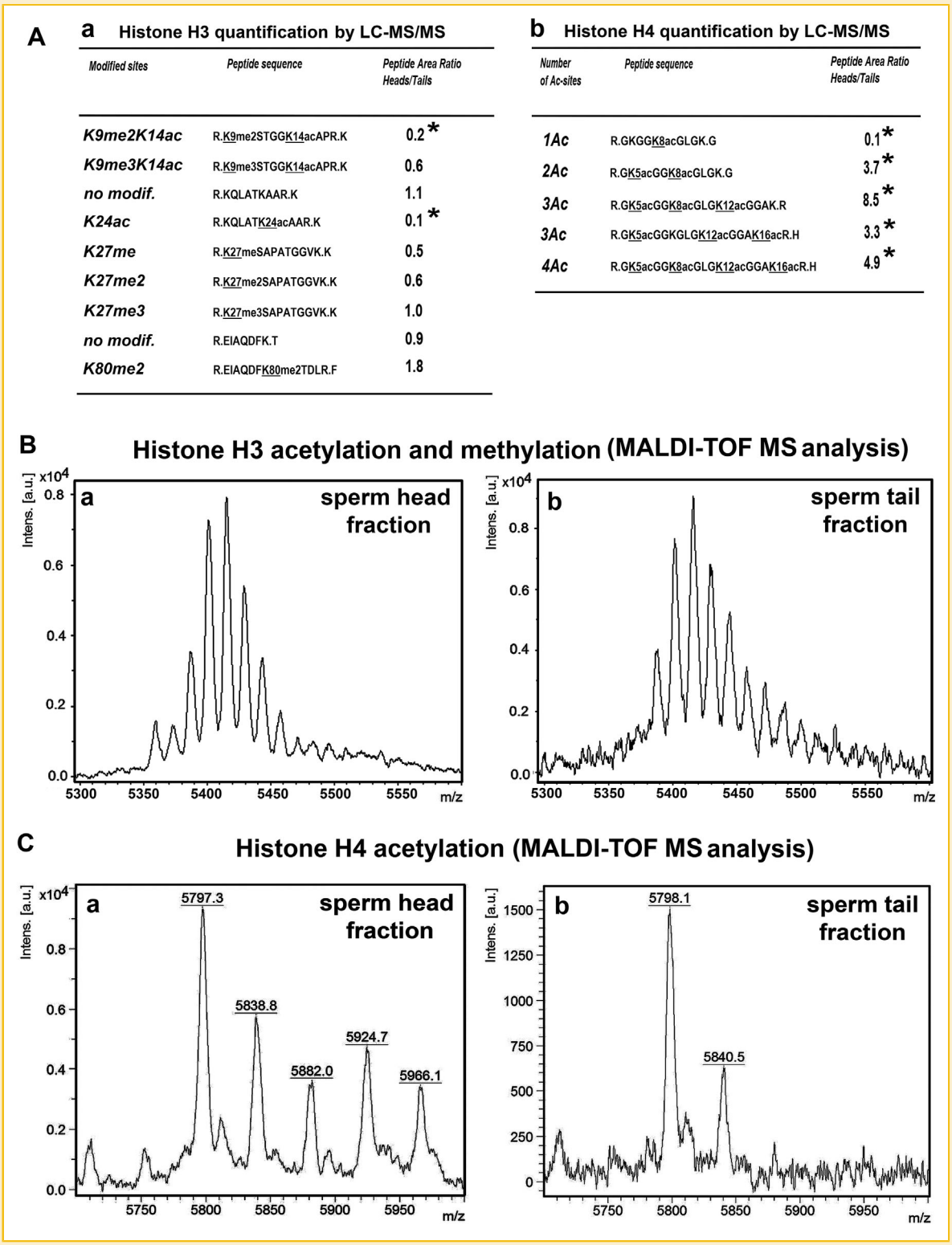

Fig. 4. LC-MS/MS analysis and MALDI-TOF MS analysis of histone H3 and H4 N-terminal peptides in human sperm head and tail fractions. A: Quantification of post-translationally modified histones (a) H3 and (b) H4, analyzed by LC-MS/MS. B: Representative MALDI-TOF MS spectra for histone H3 N-terminal peptides documenting different statuses of histone H3 modifications in the sperm (a) head and (b) tail fractions. C: MALDI-TOF MS spectra for histone H4 N-terminal peptides showing different acetylation statuses of histone H4 in the sperm (a) head and (b) tail fractions. Significant changes of peptide abundance are indicated by asterisks.

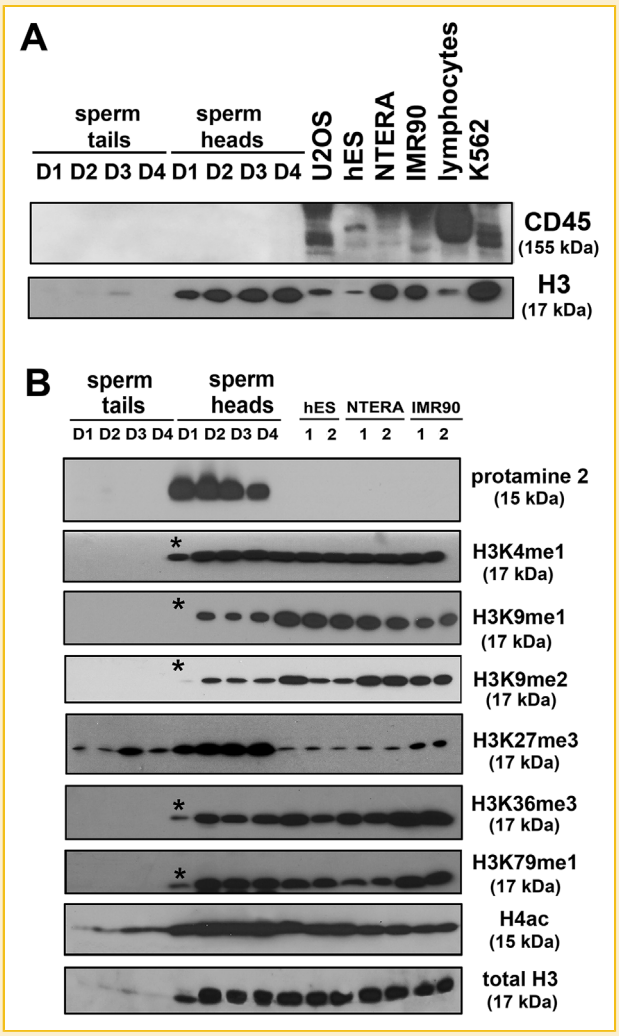

Fig. 5. Levels of protamines and post-translationally modified histones in sperm head and tail fractions. Western blot analysis was performed with lysates of human sperm head and tail fractions from four normospermic volunteers (samples D1–D4). For comparison, protein lysates from hESCs and NTERA, U2OS, IMR90, and K562 cells, and human lymphocytes were analyzed. A: Levels of CD45 (155 kDa) and histone H3 in sperm head and tail fractions. Fractions were analyzed for the presence of CD45 to detect possible somatic cell contamination. B: Levels of P2 (detected band of 15 kDa) and levels of post-translationally modified histones were normalized to those of total protein and histone H3 in the sperm head and tail fractions. The following post-translationally modified histones were studied: H3K4me1 (17 kDa), H3K9me1 (17 kDa), H3K9me2 (17 kDa), H3K27me3 (17 kDa), H3K36me3 (17 kDa), H3K79me1 (17 kDa), and H4ac (15 kDa). Asterisks show lower protein levels.

H3K9me1 (Fig. 6B). Similar to the four normospermic donors (Fig. 5B), both H4ac and H3K27me3 were present in the tail fraction of the sperm from the volunteers (Fig. 6C). To exclude the possibility of somatic cell infiltration into the tail fraction, we tested these samples for the presence of CD45 via western blot analysis (Fig. 6D, E). CD45 positivity was detected in human peripheral blood lymphocytes, and a faint band was detected in K562 leukemia cells (Fig. 6D, E), whereas the sperm head and tail fractions were CD45 negative. In addition, we studied the levels of H3K36me3 or H3K79me1 and heterogeneity in the levels of these histone markers in sperm head fractions was also observed among individuals (Figs. 5B, 6D).

CORRELATION BETWEEN P2 LEVELS AND POST-TRANSLATIONALLY MODIFIED HISTONES IN HUMAN SPERM

Using a regression analysis of the densities of western blot bands, we investigated whether a correlation exists between the levels of P2 and selected PTMs of histones (Fig. 7). Intriguingly, the level of P2 in sperm heads was positively correlated with the levels of H3K9me1, H3K9me2, H3K9ac, and H3K27me3 (Fig. 7A–D). All the histone level data reported in Figure 7 were normalized to the levels of total proteins and histone H3. More precisely, in the sperm head fraction, the regression analysis indicated that the highest correlation was between the levels of P2 and H3K9me2 ($r^2 = 0.7426$, $n = 13$) (Fig. 7A). The P2 level was also correlated with the levels of H3K9me1 ($r^2 = 0.6999$), H3K9ac ($r^2 = 0.6683$), and H2K27me3 ($r^2 = 0.5780$) (Fig. 7B–D). As other groups [Rybar et al., 2011] have done, we also investigated the effect of donor age on sperm properties. We found no correlation between donor age and the level of P2 ($r^2 = 0.0155$; Fig. 7E) or between age and the level of H3K9me2 ($r^2 = 0.0709$; Fig. 7F). We further investigated possible correlations between the level of H3K9me2 and ejaculate volume, cellularity, and sperm viability; no correlations were found in any of the cases tested (Fig. 7G–I).

In summary, a high level of protamine P2 was observed at the periphery of human sperm heads. Both P2 protamines and a substantial percentage of acetylated H4 histones bind to DNA and thus represent functional parts of the sperm genome (Fig. 3A–D). The post-translationally modified histones studied had specific morphologies (the histones appeared to be concentrated into dense strips or disk-like structures). Moreover, H3K27me3 and H4ac were present not only in sperm heads but also in sperm tails. Our additional analyses indicated that the strongest correlation exists between the levels of P2 and H3K9me2; such measurements might serve as an interesting diagnostic specification when evaluating normospermia in humans.

DISCUSSION

Interactions between protamines and sperm DNA facilitate the highest level of chromatin condensation. Protamine-bound DNA in sperm is 6–20-fold more condensed than chromatin consisting only of nucleosomes, which are formed by histones and DNA (reviewed in [Jenkins and Carrell, 2012]). Moreover, post-translationally modified residual histones in sperm chromatin serve as an epigenetic template, which may be a source of epigenetic memory for subsequent generations. In this study, we observed high levels of H3K4me1, H3K9me1, H3K9me2, H3K27me3, and H4ac in human sperm, and these observations are consistent with a MS analysis of post-translationally modified histones in mouse sperm [Brunner et al., 2014]. The presence of H3K4me1 in human sperm and the variable localization of post-translationally modified histones in sperm heads indicate that epigenomic variability exists not only among the sperm within a single sample but also among samples from different individuals. Furthermore, lifestyle-induced epigenomic instability in sperm may be an underlying cause of increasing

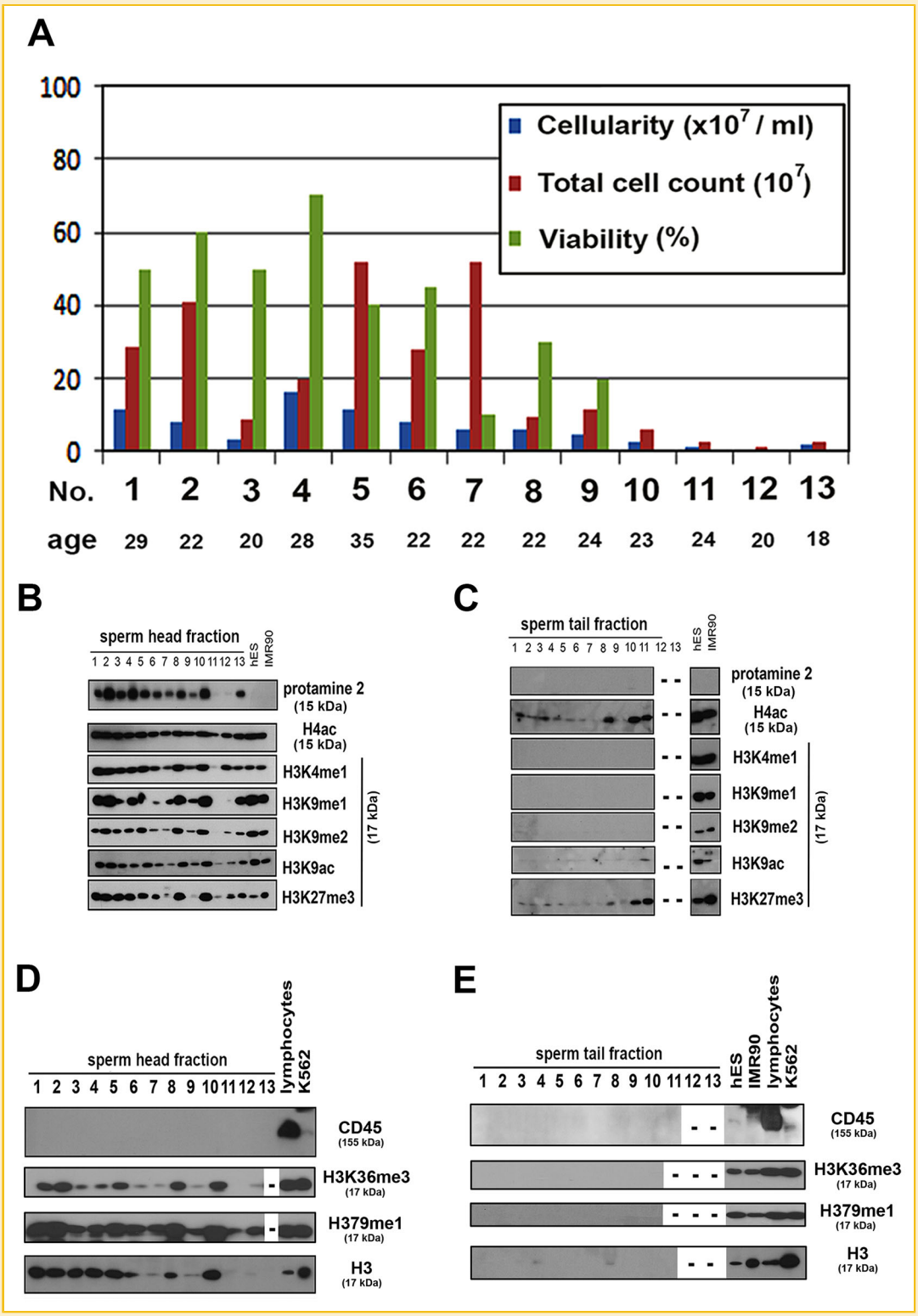

Fig. 6. Sperm characteristics and variability in the levels of protamine P2 and post-translationally modified histones. A: Cellularity, total cell count, and sperm viability were analyzed in the sperm from 13 volunteers. B–C: Levels of P2 (15 kDa) and selected modified histones (H4ac, H3K4me1, H3K9me1, H3K9me2, H3K9ac, and H3K27me3; all 17 kDa MW) in the sperm (B) head and (C) tail fractions. Equal amounts of total protein were loaded. The data were compared to level of total histone H3 (17 kDa) shown in panels D and E. Panels D–E: Potential contamination in the sperm head and tail fractions with material from the somatic cell fraction was examined by blotting with anti-CD45 (band size was 155 kDa). Panels also show levels of H3K36me3 (17 kDa) and H3K79me1 (17 kDa) in human sperm.

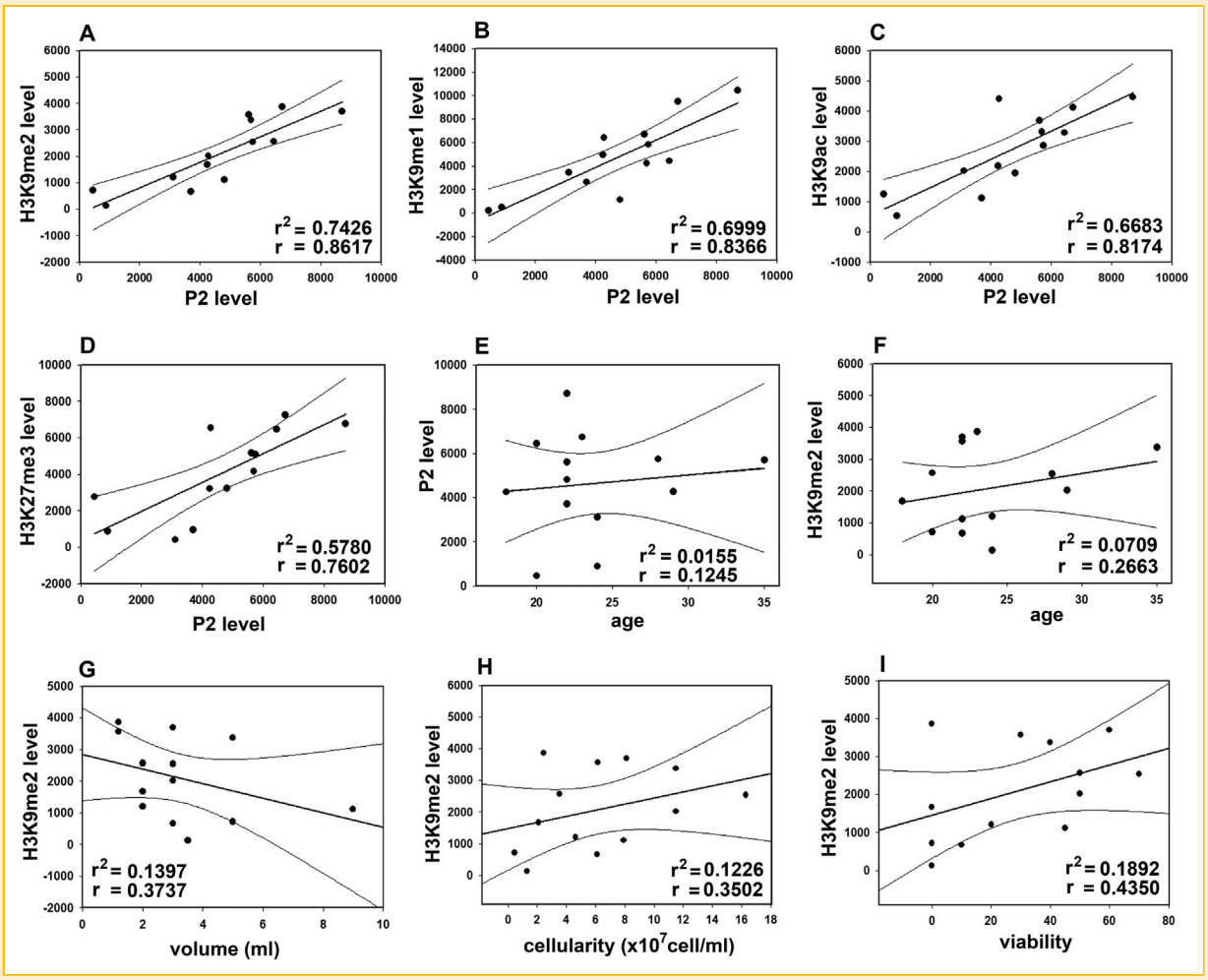

Fig. 7. Correlation analyses of the relationships between sperm properties. Correlation analyses were performed to assess the relationships between the levels of P2 and those of the following: A: H3K9me2, B: H3K9me1, C: H3K9ac, and D: H3K27me3. A correlation between the P2 and H3K9me2 levels was found (Pearson's correlation coefficient: $r^2 = 0.7426$). Linear regression analyses revealed correlations between the P2 level and the levels of H3K9me1 ($r^2 = 0.6999$), H3K9ac ($r^2 = 0.6683$), and H3K27me3 ($r^2 = 0.5780$). $N = 13$; $P \leq 0.01$ for all. In the graphs, 95% confidence intervals are shown. Regression analyses showed no correlation between the following: E: P2 level and donor age ($r^2 = 0.0155$) or F: H3K9me2 level and donor age ($r^2 = 0.0709$). The results of the regression analyses are shown for H3K9me2 level and G: sperm volume, H: ejaculate cellularity, and I: sperm viability.

male infertility. We also observed in our investigation that at least H4ac and H3K27me3 may appear in the mid-piece and remainder of tails in human sperm, which is an unexpected finding (Figs. 2, 4A–C, 5B and 6C). We found occurrence of residual histones in the mitochondria-containing mid-piece, which may explain this phenomenon, even though mitochondrial DNA is histone-free [Jansen, 2000]. The sperm mid-piece contains 17 kDa mitochondrial capsule selenoproteins [Brown and Arthur, 2001]; therefore, the occurrence of histones in the mid-piece and in the remainder of the sperm tails is remarkable. We verified this phenomenon using four independent approaches. (1) An immunofluorescence analysis revealed modified histones (H3K27me3 and H4ac) in sperm tails (Fig. 2Ba, Bb, Ca, Cb); however, this finding could have been due to the nonspecific binding of antibodies or the autofluorescence of cellular structures. Therefore, we used an additional experimental approach. (2) Western blot analyses were positive for H3K27me3 and H4ac in the sperm tail fractions (Figs. 5B and 6C). If fraction leakage had occurred, all of the modified histones that were analyzed, including H3K4me1, H3K9me1/me2, H3K36me3 and H3K79me1, would have been detected in the sperm tails, but this was not the case (Figs. 5B and 6C, E). (3) We also performed LS-MS/MS and MALDI-TOF MS analysis of PTMs of histones H3 and H4 (Fig. 4A–C), which confirmed the presence of histones in the sperm tail fraction. (4) The possible infiltration of somatic cells (e.g., lymphocytes) into the sperm head and tail fractions during the separation procedure was tested using western blot analysis of CD45 positivity. The tail fraction was negative for this marker (Figs. 5A and 6E). Together, our analyses demonstrated that the sperm tail fraction contains residual histones with specific PTMs. Our data indicating that H4ac and H3K27me3 exist not only in the nuclear pool but also in sperm tails (Figs. 5B, and 6C) fits well with the results of Pinheiro et al. [2012], who found H3K9me1 in the cytoplasmic pool of immortalized mouse

embryonic fibroblasts. Histones, as detected in Figure 6C, must be non-integrated, residual, and likely useless sperm components that cannot participate in paternal epigenetic memory. However, because the whole sperm enters the oocyte, it is not possible to completely exude that post-translationally modified histones of sperm tails cannot serve as a template for the chromatin of the zygote. If this is not the case, the question remains how these residual histones are eliminated from the cytoplasm of gametes or zygotes. Mechanisms may be similar to those described for the elimination of paternal mitochondrial DNA, which occurs after fertilization, such as degradation by a specific nuclease-dependent system, a ubiquitin-proteasome system or autophagy (summarized by Sato and Sato [2012]).

While paternal epigenetic memory and the subsequent epigenetic reprogramming of the zygote can be mediated by residual, post-translationally modified histones in the sperm head fraction, the status of protamines, including protamine phosphorylation and acetylation, may also contribute to this process, as described by Brunner et al. [2014]. As we found, there is a strong correlation between the levels of P2 and H3K9me2 (Fig. 7A). Therefore, we believe that our experimental approach demonstrates the importance of analyzing not only protamines but also histones with PTMs in sperm. This finding could be of potential interest to clinical laboratories because histone PTMs appear to be important markers of the physiological conditions of the sperm (Figs. 6A–E, 7A–D). Equally important conclusions were drawn by Benchaib et al. [2005] with respect to sperm DNA methylation. These authors demonstrated that nonstandard levels of sperm DNA methylation did not influence in vitro fertilization but significantly influenced embryonic development. It is well known that DNA of infertile men is characterized by disordered DNA methylation. Notably, a negative correlation was found between sperm DNA methylation and the DNA damage caused by oxidative stress [Tunc and Tremellen, 2009]. A positive correlation was found between DNA integrity in sperm and DNA integrity in the leukocytes of identical donors [Babazadeh et al., 2010]. Thus, one of the etiologies underlying male infertility is sperm DNA damage [Tunc and Tremellen, 2009; Babazadeh et al., 2010]. Based on the results of the aforementioned experiments, it is evident that studies of genomic and epigenomic stability/instability in sperm are required to understand the molecular underpinnings of male infertility.

Protamines and PTMs of histones represent important epigenetic features that could serve as markers of male fertility. Thus, correlation analyses of the levels of protamines and post-translationally modified histones might represent additional diagnostic criteria in clinical laboratories. An important question in the field of chromatin biology is whether specifically modified sperm histones (in comparison to protamines) associate with specific DNA sequences or are distributed randomly in the sperm nucleus [Gatewood et al., 1987; Ward, 2010]. For example, Arpanahi et al. [2009] demonstrated that sperm histones are primarily associated with gene promoters. Similarly, Hammoud et al. [2011] reported that histones are distributed non-randomly in sperm chromatin and associate only with specific genes. This observation is in accord with the nonrandom positioning of histone markers on non-randomly located chromosomes in sperm heads [Manvelyan et al., 2008]. In this study, we demonstrated that considerable variability exists in post-translationally modified histones in individual sperm, and unique localization patterns were observed, in particular for H3K4me1 and H3K27me3 (Fig. 2Aa, Ab and Ba, Bb, yellow arrows). In some sperm heads, modified histones H3 and H4 were homogeneously distributed, but in other sperm heads, these modified histones accumulated in discrete regions (Fig. 2). Similarly, both focal and diffuse immunofluorescence signals for histone H2B were observed in human sperm by Zini et al. [2008]. In our investigation, we found strips or disk-like localization patterns for modified histones and high concentrations of protamines very close to the periphery of the sperm nucleus (Figs. 1A, B). These results indicate that the compartmentalization of epigenetic markers occurs in human sperm.

Advanced proteomics methods, including MS and western blot analysis, have the potential to reveal novel PTMs on histone tails and protamines. These methods can also be applied to the analysis of the sperm proteome and, in particular, the precise characterization of protamines and histones, the disrupted function of which must be taken into account in the context of human infertility [Brunner et al., 2014]. In this report, we demonstrated that H3K9 methylation and acetylation levels can be important markers of human sperm quality, especially when a correlation analysis is performed with respect to the protamine P2 levels. Therefore, attention should also be paid to the modulation of the epigenetic status of histones, protamines, and sperm DNA. From this point of view, dietary factors represent an interesting aspect of epigenetics. For example, the application of natural products (e.g., curcumin, resveratrol, or butyrate) and their synthetic analogs as "epi-drugs" that act as small molecule inhibitors of histone acetyl transferases (HATs) or histone deacetylases (HDACs) may have the potential to change the sperm epigenome and impact male fertility [Choi and Friso, 2010]. A similar suggestion has been made previously [Balhorn, 2007] regarding antioxidant supplementation, which may have the potential to reduce DNA damage in sperm and normalize the level of sperm DNA methylation, the disorder of which unambiguously affects sperm quality [Benchaib et al., 2005; Tunc and Tremellen, 2009].

ACKNOWLEDGMENTS

We thank Ing. Vladimír Kopřiva for sample fixation and Dr. Roman Rybář of the IVF clinic Sanus Jihlava for the analysis of normospermia according to the WHO 2010 criteria. The authors declare no conflicts of interest. A linguistics revision was performed by a native speaker from American Journal Experts (AJE, USA).

REFERENCES

Aoki VW,Emery BR, Liu L, Carrell DT. 2006. Protamine levels vary between individual sperm cells of infertile human males and correlate with viability and DNA integrity. J Androl 27:890–898.

Armbruster BL, Wunderli H, Turner BM, Raska I, Kellenberger E. 1983. Immunocytochemical localization of cytoskeletal proteins and histone 2B in isolated membrane-depleted nuclei, metaphase chromatin, and whole Chinese hamster ovary cells. J Histochem Cytochem 31:1385–1393.

Arpanahi A, Brinkworth M, Iles D, Krawetz SA, Paradowska A, Platts AE, Saida M, Steger K, Tedder P, Miller D. 2009. Endonuclease-sensitive regions of human spermatozoal chromatin are highly enriched in promoter and CTCF binding sequences. Genome Res 19:1338–1349.

Baarends WM, Hoogerbrugge JW, Roest HP, Ooms M, Vreeburg J, Hoeijmakers JH, Grootegoed JA. 1999. Histone ubiquitination and chromatin remodeling in mouse spermatogenesis. Dev Biol 207:322–333.

Baarends WM, van der Laan R, Grootegoed JA. 2000. Specific aspects of the ubiquitin system in spermatogenesis. J Endocrinol Invest 23:597–604.

Babazadeh Z, Razavi S, Tavalaee M, Deemeh MR, Shahidi M, Nasr-Esfahani MH. 2010. Sperm DNA damage and its relation with leukocyte DNA damage. Reprod Toxicol 29:120–124.

Balhorn R. 2007. The protamine family of sperm nuclear proteins. Genome Biol 8:227.

Bannister AJ, Kouzarides T. 2011. Regulation of chromatin by histone modifications. Cell Res 21:381–395.

Bartova E, Kozubek S, Jirsova P, Kozubek M, Lukasova E, Skalnikova M, Cafourkova A, Koutna I, Pasekova R. 2001. Higher-order chromatin structure of human granulocytes. Chromosoma 110:360–370.

Bartova E, Harnicarova A, Pachernik J, Kozubek S. 2005. Nuclear topography and expression of the BCR/ABL fusion gene and its protein level influenced by cell differentiation and RNA interference. Leuk Res 29:901–913.

Benchaib M, Braun V, Ressnikof D, Lornage J, Durand P, Niveleau A, Guerin JF. 2005. Influence of global sperm DNA methylation on IVF results. Hum Reprod 20:768–773.

Brown KM, Arthur JR. 2001. Selenium, selenoproteins and human health: a review. Public Health Nutr 4:593–599.

Brunner AM, Nanni P, Mansuy IM. 2014. Epigenetic marking of sperm by post-translational modification of histones and protamines. Epigenetics Chromatin 7:2.

Carrell DT. 2012. Epigenetics of the male gamete. Fertil Steril 97:267–274.

Carrell DT, Emery BR, Hammoud S. 2008. The aetiology of sperm protamine abnormalities and their potential impact on the sperm epigenome. Int J Androl 31:537–545.

Cincarova L, Lochmanova G, Novakova K, Sultesova P, Konecna H, Fajkusova L, Fajkus J, Zdrahal Z. 2012. A combined approach for the study of histone deacetylase inhibitors. Mol Biosyst 8:2937–2945.

Choi SW, Friso S. 2010. Epigenetics: a new bridge between nutrition and health. Adv Nutr 1:8–16.

Emery BR, Carrell DT. 2006. The effect of epigenetic sperm abnormalities on early embryogenesis. Asian J Androl 8:131–142.

Gatewood JM, Cook GR, Balhorn R, Bradbury EM, Schmid CW. 1987. Sequence-specific packaging of DNA in human sperm chromatin. Science 236:962–964.

Govin J, Lestrat C, Caron C, Pivot-Pajot C, Rousseaux S, Khochbin S. 2006. Histone acetylation-mediated chromatin compaction during mouse spermatogenesis. Ernst Schering Res Found Workshop 57:155–172.

Hammadeh ME, Hamad MF, Montenarh M, Fischer-Hammadeh C. 2010. Protamine contents and P1/P2 ratio in human spermatozoa from smokers and non-smokers. Hum Reprod 25:2708–2720.

Hammoud SS, Nix DA, Hammoud AO, Gibson M, Cairns BR, Carrell DT. 2011. Genome-wide analysis identifies changes in histone retention and epigenetic modifications at developmental and imprinted gene loci in the sperm of infertile men. Hum Reprod 26:2558–2569.

Jansen RP. 2000. Origin and persistence of the mitochondrial genome. Hum Reprod 15(Suppl2):1–10.

Jenkins TG, Carrell DT. 2012. Dynamic alterations in the paternal epigenetic landscape following fertilization. Front Genet 3:143.

Jenuwein T, Allis CD. 2001. Translating the histone code. Science 293: 1074–1080.

Korrodi-Gregório L, Ferreira M, Vintém AP, Wu W, Muller T, Marcus K, Vijayaraghavan S, Brautigan DL, da Cruz E, Silva OA, Fardilha M, da Cruz E, Silva EF. 2013. Identification and characterization of two distinct PPP1R2 isoforms in human spermatozoa. BMC Cell Biol 14:15.

Kouzarides T. 2007. Chromatin modifications and their function. Cell 128:693–705.

Kuretake S, Kimura Y, Hoshi K, Yanagimachi R. 1996. Fertilization and development of mouse oocytes injected with isolated sperm heads. Biol Reprod 55:789–795.

Lee CH, Cho YH. 1999. Aspects of mammalian spermatogenesis: electrophoretical analysis of protamines in mammalian species. Mol Cells 9: 556–559.

Lee K, Haugen HS, Clegg CH, Braun RE. 1995. Premature translation of protamine 1 mRNA causes precocious nuclear condensation and arrests spermatid differentiation in mice. Proc Natl Acad Sci U S A 92:12451–12455.

Legartova S, Kozubek S, Franek M, Zdrahal Z, Lochmanova G, Martinet N, Bartova E. 2014. Cell differentiation along multiple pathways accompanied by changes in histone acetylation status. Biochem Cell Biol 92:85–93.

Luco RF, Pan Q, Tominaga K, Blencowe BJ, Pereira-Smith OM, Misteli T. 2010. Regulation of alternative splicing by histone modifications. Science 327:996–1000.

Manvelyan M, Hunstig F, Bhatt S, Mrasek K, Pellestor F, Weise A, Simonyan I, Aroutiounian R, Liehr T. 2008. Chromosome distribution in human sperm – a 3D multicolor banding-study. Mol Cytogenet 1:25.

Meistrich ML, Trostle-Weige PK, Lin R, Bhatnagar YM, Allis CD. 1992. Highly acetylated H4 is associated with histone displacement in rat spermatids. Mol Reprod Dev 31:170–181.

Morris ID, Ilott S, Dixon L, Brison DR. 2002. The spectrum of DNA damage in human sperm assessed by single cell gel electrophoresis (Comet assay) and its relationship to fertilization and embryo development. Hum Reprod 17: 990–998.

Pinheiro I, Margueron R, Shukeir N, Eisold M, Fritzsch C, Richter FM, Mittler G, Genoud C, Goyama S, Kurokawa M. 2012. Prdm3 and Prdm16 are H3K9me1 methyltransferases required for mammalian heterochromatin integrity. Cell 5:948–960.

Polo SE, Jackson SP. 2011. Dynamics of DNA damage response proteins at DNA breaks: a focus on protein modifications. Genes Dev 25:409–433.

Rice JC, Allis CD. 2001. Histone methylation versus histone acetylation: new insights into epigenetic regulation. Curr Opin Cell Biol 13:263–273.

Rohlf JF, Sokal RR. 1993. Statistical Tables. New York: W.H. Freeman and Company.

Rybar R, Kopecka V, Prinosilova P, Markova P, Rubes J. 2011. Male obesity and age in relationship to semen parameters and sperm chromatin integrity. Andrologia 43:286–291.

Sato M, Sato K. 2012. Maternal inheritance of mitochondrial DNA: Degradation of paternal mitochondria by allogeneic organelle autophagy, allophagy. Autophagy 8:424–425.

Taddei A, Roche D, Bickmore WA, Almouzni G. 2005. The effects of histone deacetylase inhibitors on heterochromatin: implications for anticancer therapy?. EMBO Rep 6:520–524.

Tunc O, Tremellen K. 2009. Oxidative DNA damage impairs global sperm DNA methylation in infertile men. J Assist Reprod Genet 26:537–544.

van der Heijden GW, Ramos L, Baart EB, van den Berg IM, Derijck AA, van der Vlag J, Martini E, de Boer P. 2008. Sperm-derived histones contribute to zygotic chromatin in humans. BMC Dev Biol 8:34.

Ward WS. 1993. Deoxyribonucleic acid loop domain tertiary structure in mammalian spermatozoa. Biol Reprod 48:1193–1201.

Ward WS, Kishikawa H, Akutsu H, Yanagimachi H, Yanagimachi R. 2000. Further evidence that sperm nuclear proteins are necessary for embryogenesis. Zygote 8:51–56.

Ward WS. 2010. Function of sperm chromatin structural elements in fertilization and development. Mol Hum Reprod 16:30–36.

Zalensky AO, Breneman JW, Zalenskaya IA, Brinkley BR, Bradbury EM. 1993. Organization of centromeres in the decondensed nuclei of mature human sperm. Chromosoma 102:509–518.

Zalensky AO, Siino JS, Gineitis AA, Zalenskaya IA, Tomilin NV, Yau P, Bradbury EM. 2002. Human testis/sperm-specific histone H2B (hTSH2B). Molecular cloning and characterization. J Biol Chem 277:43474–43480.

Zini A, Zhang X, San Gabriel M. 2008. Sperm nuclear histone H2B: correlation with sperm DNA denaturation and DNA stainability. Asian J Androl 10:865–871.

SUPPORTING INFORMATION

Additional supporting information may be found in the online version of this article at the publisher's web-site.